Backbone Dynamics of Chymotrypsin Inhibitor 2: Effect of Breaking the Active Site Bond and Its Implications for the Mechanism of Inhibition of Serine Proteases†

Graeme L. Shaw, Ben Davis, James Keeler,* and Alan R. Fersht*

Department of Chemistry, University of Cambridge, Lensfield Road, Cambridge CB2 1EW, United Kingdom

Received August 19, 1994; Revised Manuscript Received November 17, 1994®

ABSTRACT: The backbone dynamics of uniformly ^{15}N-labeled chymotrypsin inhibitor 2 (CI2) and of the complex formed by the association of two fragments consisting of residues 20−59 and 60−83 have been studied. A data set consisting of ^{15}N longitudinal (T_1) and transverse ($T_{1\rho}$) relaxation times and {^1H}−^{15}N NOE enhancements has been measured for all backbone NH groups in both proteins. Information on internal motions has been extracted from these data using the model-free approach to determine order parameters (S^2) and effective internal correlation times (τ_e). The data indicate that most of the backbone of CI2 is highly constrained ($S^2 \approx 0.9$) with the exception of residues in the binding loop (residues 54−64), which have slightly lower order parameters. Most of the residues in the CI2(20−59)•(60−83) complex are also highly constrained ($S^2 \approx 0.9$). However, the loss of the covalent bond between Met59 and Glu60 leads to a large increase in the mobility of residues in the loop region. The residues in the first half of the loop region have significantly lower order parameters than those in the second half of the loop. This observation suggests that the NH_2 group that is released on cleavage of the scissile bond remains anchored in its original position, inhibiting the attack of water on the acyl-enzyme that is formed between the protease and the cleaved inhibitor. More importantly, the NH_2 group is optimally placed for reversing the formation of the acyl-enzyme so that the equilibrium between the cleaved and uncleaved inhibitor, bound to the protease, greatly favors the uncleaved complex.

Chymotrypsin inhibitor 2 (CI2)[1] is a small, 83-residue, globular protein, which is a potent inhibitor of serine proteases. A proposed mechanism for the inhibitory activity of CI2 (Longstaff et al., 1990; Laskowski & Kato, 1980) has the equilibrium between the intact inhibitor bound to the protease and the acyl-enzyme intermediate strongly favoring the intact form of the inhibitor. For this equilibrium to occur, the free amine group released by the cleavage of the peptide bond must be held in a native-like position, allowing re-formation of the peptide bond and sterically hindering the associated hydrolysis reaction which would result in irreversible proteolysis of the inhibitor. The active site scissile bond, Met59−Glu60, is located in a long extended loop (residues 54−64). It has been shown previously that cleavage of this bond with CNBr produces two fragments, CI2(20−59) and CI2(60−83), which reassociate to form a highly native-like noncovalent complex, CI2(20−59)•(60−83) (Prat Gay & Fersht, 1994; Prat Gay et al., 1994). This complex is an excellent model to investigate the structure adopted by CI2 when the scissile bond is cleaved and to test this hypothesis.

With the exception for residues 1−19, which are disordered in solution and do not contribute to the stability of the protein, CI2 is highly structured, consisting of a region of mixed parallel and antiparallel β-sheet and a single α-helix (McPhalen & James, 1987; Ludvigsen et al., 1991). In this work, a truncated version of CI2, CI2(20−83), was used (Jackson et al., 1993; Osmark et al., 1993), which does not contain the disordered N-terminal region; the structure of this construct is shown in Figure 1. For convenience, no distinction is made between CI2 and the truncated version of CI2 in the following discussion.

In this paper, we present a study of the backbone dynamics of CI2 and of the CI2(20−59)•(60−83) complex. The study of backbone dynamics, through the measurement of ^{15}N relaxation data, has allowed us to investigate the effect of breaking the active site bond on the rigidity of the CI2 structure. The results of these studies have been interpreted in terms of the mechanism of inhibition of serine proteases by CI2.

Relaxation Theory. The two major sources of relaxation for ^{15}N nuclei in proteins are the dipolar coupling with the attached proton and the anisotropy of the ^{15}N chemical shift. If cross-correlation between these two relaxation mechanisms is ignored, the longitudinal relaxation time, T_1, the transverse relaxation time, T_2, and the steady-state NOE enhancement, η, are given by (Abragam, 1961)

$$R_1 = \frac{1}{T_1} = \frac{1}{4}d^2\{J(\omega_H - \omega_N) + 3J(\omega_N) + 6J(\omega_H + \omega_N)\} + \frac{1}{3}c^2J(\omega_N) \quad (1)$$

† Contribution from the MRC Unit for Protein Function and Design and the Cambridge Centre for Protein Engineering. G.L.S. thanks The Cambridge Commonwealth Trust for financial assistance, and B.D. has an MRC studentship.

* Author to whom correspondence should be addressed.

® Abstract published in *Advance ACS Abstracts,* February 1, 1995.

[1] Abbreviations: CI2, chymotrypsin inhibitor 2; NMR, nuclear magnetic resonance; T_1, longitudinal relaxation time; T_2, transverse relaxation time; NOE, nuclear Overhauser effect; $T_{1\rho}$, longitudinal relaxation time in the rotating frame; FID, free induction decay; F_1, first frequency dimension; F_2, second frequency dimension; TPPI, time-proportional phase incrementation; t_1, first dimension incremental delay.

0006-2960/95/0434-2225$09.00/0

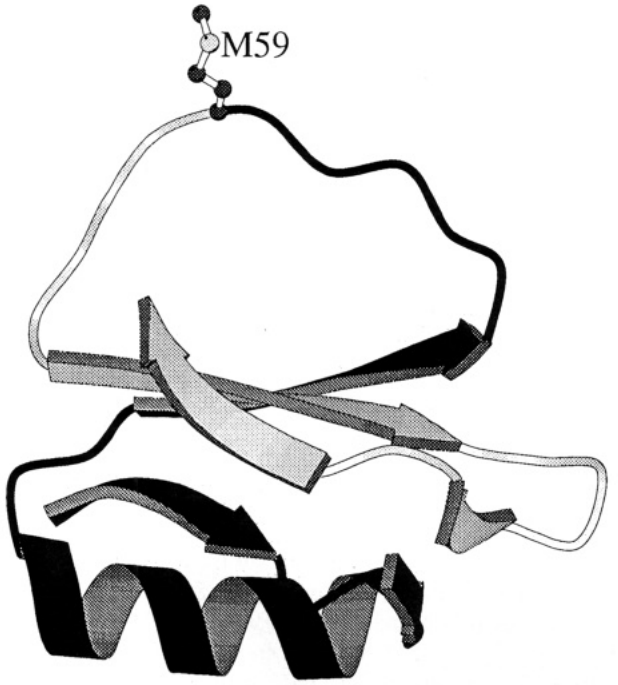

FIGURE 1: MOLSCRIPT diagram (Kraulis, 1991) of the structure of CI2 showing the position of the loop region relative to the core of the protein. Residues 20−59 are indicated by darker shading while residues 60−83 are indicated by lighter shading.

$$R_2 = \frac{1}{T_2} = \frac{1}{8}d^2\{4J(0) + J(\omega_H - \omega_N) + 3J(\omega_N) + 6J(\omega_H) + 6J(\omega_H + \omega_N)\} + \frac{1}{18}c^2\{3J(\omega_N) + 4J(0)\} + R_{ex} \quad (2)$$

$$\eta = \frac{1}{4}\frac{\gamma_H}{\gamma_N}d^2\{6J(\omega_H + \omega_N) - J(\omega_H - \omega_N)\}T_1 \quad (3)$$

Here $d = \gamma_H\gamma_N h(\mu_0/4\pi)(1/r_{NH}^3)$ and $c = \omega_N(\sigma_\parallel - \sigma_\perp)$; γ_H and γ_N are the gyromagnetic ratios of ^{1}H and ^{15}N (2.6752×10^8 and -2.7108×10^7 rad s^{-1} T^{-1}, respectively); ω_H and ω_N are the Larmor frequencies of ^{1}H and ^{15}N (3.1428×10^9 and -3.185×10^8 rad s^{-1}, respectively, at 11.8 T), r_{NH} is the N−H bond length (taken here as 1.03 Å), and $J(\omega_i)$ are the spectral densities at the angular frequency ω_i. An axially symmetric chemical shift tensor has been assumed for ^{15}N with $(\sigma_\parallel - \sigma_\perp) = -160$ ppm (Hiyama et al., 1988). R_1 and R_2 are the reciprocals of T_1 and T_2 and are the longitudinal and transverse relaxation rate constants. In addition, random variation in the isotropic chemical shift of ^{15}N may contribute to the transverse relaxation of ^{15}N. In proteins, such variations are due to slow conformational exchange, and under some circumstances, they may make significant contributions to the transverse relaxation rate. This contribution to T_2 is called the exchange contribution and is represented as R_{ex} in eq 2.

The spectral density function in eqs 1−3 is likely to depend on the overall correlation time for molecular tumbling as well as the nature and rate of any internal motions which may be occurring. The measurement of only three relaxation parameters for each residue is insufficient to characterize these motions in detail, and so an approximate spectral density function is needed; the "model-free" approach (Lipari & Szabo, 1982a,b) provides a convenient and useful approximation for $J(\omega_i)$. The Lipari and Szabo model characterizes the internal motions in terms of a generalized order parameter, S^2 ($0 \le S^2 \le 1$), and an internal correlation time, τ_e. The order parameter indicates the extent of restriction of internal motion; a value of 0 implies the internal motion is completely free, while a value of 1 indicates that there is no internal motion. The internal correlation time is an indicator of the rate of these motions. The Lipari and Szabo approach uses the following spectral density function:

$$J(\omega) = \frac{2}{5}\left(\frac{S^2\tau_M}{1 + \omega^2\tau_M^2} + (1 - S^2)\frac{\tau}{1 + \omega^2\tau^2}\right) \quad (4)$$

where τ_M is the correlation time for overall tumbling and $\tau^{-1} = \tau_M^{-1} + \tau_e^{-1}$; S^2 and τ_e are different for each residue while τ_M is fixed for the whole protein.

Having measured a set of relaxation parameters, the order parameters and internal correlation times are determined by minimizing the function

$$\chi_i^2 = \frac{(R_{1i} - R_{1i}^c)^2}{\sigma_{1i}^2} + \frac{(R_{2i} - R_{2i}^c)^2}{\sigma_{2i}^2} + \frac{(\eta_i - \eta_i^c)^2}{\sigma_{\eta_i}^2} \quad (5)$$

where the index, i, indicates that the values are taken for residue number i; σ_{1i}^2, σ_{2i}^2, and $\sigma_{\eta_i}^2$ are the variances in the experimental relaxation parameters R_{1i}, R_{2i}, and η_i, respectively. The calculated parameters R_{1i}^c, R_{2i}^c, and η_i^c are determined by using trial values of the model parameters in eqs 1−3, and the optimum values of these parameters are found by minimizing χ_i^2 using a suitable nonlinear method, for example, the Levenberg−Marquardt algorithm (Press et al., 1992). A separate minimization is performed for each residue.

A value for the correlation time for overall tumbling is needed before S^2 and τ_e can be found. It has been shown (Kay et al., 1989) that provided that τ_e is short enough and that there is no exchange contribution to T_2, the ratio T_1/T_2 is independent of both S_2 and τ_e; under these circumstances the average T_1/T_2 ratio can be used to obtain an initial estimate of τ_M. Initially the relaxation data were analyzed using a model with no exchange contribution to T_2. If, however, this model was unable to reproduce the observed T_2 within the limits of experimental error, an exchange contribution was included. Since there are just three measured relaxation parameters for each residue, extending the model to include more than three parameters (S^2, τ_e, R_{ex}) is not justifiable.

In this work, it is desirable to be able to compare the absolute sizes of the order parameters for each protein. For such a comparison to be free of systematic error, the value of τ_M used to determine model parameters must be estimated as reliably as possible. The initial estimate for τ_M, obtained from the T_1/T_2 ratio, can be optimized by first minimizing χ_i^2 for each residue and calculating an overall χ^2 by summing χ_i^2 over all the residues in the protein. A grid search can then be performed on τ_M until the overall χ^2 is minimized, leading to an optimized value of τ_M. Clearly the grid search cannot change the value of τ_M too much without causing a large increase in χ^2; to make a large change in τ_M without causing a large change in χ^2, the model for internal motion must be able to change, *e.g.*, by allowing the number of exchange contributions to vary. Since the initial estimate of τ_M fixes the models for internal motion

for each residue, this approach will clearly work best when the initial estimate of τ_M is close to the true τ_M. This should be achieved in this work since the T_1/T_2 ratio is fairly constant across the protein sequence both for CI2 and for CI2(20−59)•(60−83), making the initial estimate of τ_M quite reliable.

Although this work will discuss the mobility of different residues, clearly the discussion is limited to the backbone mobility. Information concerning side-chain mobility would require additional measurements.

EXPERIMENTAL PROCEDURES

Sample Preparation. Uniformly ^{15}N-labeled CI2 and CI2-(20−59)•(60−83) were expressed and purified as to be described elsewhere (B. Davis, G. Prat Gay, and A. R. Fersht, unpublished). Both proteins were lyophilized and dissolved in 500 μL of 50 mM sodium acetate-d_3 (pH 4.6) in 9:1 H_2O:D_2O. Samples contained 2 mM protein.

NMR Spectroscopy. All relaxation experiments were performed at 25 °C on a Bruker AMX500 spectrometer operating at a frequency of 500.13 MHz for ^{1}H. The ^{15}N T_1 and $T_{1\varrho}$ relaxation times were measured using the pulse sequences described previously (van Mierlo, 1993). For both experiments, a total recycle delay of 3 s was used, which was approximately 5 times the longest T_1 of the NH protons. During 2 s of this period, low-power presaturation of the water resonance was used. For the $T_{1\varrho}$ experiment, the ^{15}N magnetization was spin-locked using a field strength of 4.3 kHz; for the range of offsets in the ^{15}N spectrum this field locks the corresponding magnetization about an axis within ±7° of the transverse plane. Under these circumstances and in the absence of low-frequency perturbations, $T_{1\varrho}$ should be equivalent to T_2. From this point, we shall drop the distinction between $T_{1\varrho}$ and T_2 and refer to the measured transverse relaxation times simply as T_2.

The {^{1}H}−^{15}N NOE enhancements were measured using a sensitivity-enhanced sequence (Palmer et al., 1991; Stone et al., 1992) that allows two ^{1}H−^{15}N correlation spectra to be measured simultaneously and hence can give two estimates of the NOE enhancement. In the NOE experiments, water suppression was achieved by applying two orthogonal purge pulses, of duration 5 ms at full power, just prior to the first 90° ^{15}N pulse. A recycle delay of 3 s, which was approximately 5 times the longest T_1 for ^{15}N, was used. WALTZ-16 decoupling (Shaka et al., 1983) was applied during this delay for the NOE experiment.

In all experiments, the spectral widths were 8064 and 1774 Hz in the ^{1}H and ^{15}N dimensions, respectively. A total of 1024 complex points were collected in t_2 giving an acquisition time of 127 ms; in t_1 400 real points were collected giving a maximum t_1 of 113 ms. For CI2, the T_1 experiment employed a total of nine relaxation delays (5 ms, 35 ms, 80 ms, 140 ms 200 ms, 400 ms, 600 ms, 900 ms, and 1.8 s) while for the T_2 experiment seven relaxation delays were used (10 ms, 30 ms, 60 ms, 100 ms, 150 ms, 230 ms, and 350 ms). For CI2(20−59)•(60−83), the T_1 experiment contained eight relaxation delays (5 ms, 35 ms, 80 ms, 140 ms, 200 ms, 400 ms, 600 ms, and 1.0 s) while the T_2 experiment used six relaxation delays (10 ms, 30 ms, 60 ms, 100 ms, 150 ms, and 230 ms).

Data Analysis. Spectra were processed using a mild Lorentzian window function in F_2 and a cosine-bell squared window function in F_1. The contribution of the water signal to the FID was removed in the time domain, prior to the application of the window function, using a convolution difference routine (Marion et al., 1989). A linear baseline correction was applied in the F_2 dimension. For the T_1 and T_2 experiments the heights of the cross-peaks were measured at each value of the relaxation delay. These peak heights were fitted to the relation

$$I(t) = I^0 \exp(-t/T_i) \tag{6}$$

where $I(t)$ is the peak height for a relaxation time, t, and T_i is the fitted relaxation time ($i = 1, 2$). Figure 2 shows some repesentative raw data for both CI2 and the CI2(20−59)•(60−83) complex. The best fit exponential curves are also shown, and data which show an excellent, average, and poor fit to the curve have been chosen. The exponential fitting was performed using KaleidaGraph 2.1 (Abelbeck software), and the uncertainties in the relaxation times are the standard errors given by the general fitting routine. The {^{1}H}−^{15}N NOE enhancement, η, was calculated from the height of the cross-peak in the NOE, I, and the reference experiments, I_0, according to

$$\eta = \frac{I - I_0}{I_0} \tag{7}$$

The use of the sensitivity-enhanced sequence allowed two simultaneous measurements of the NOE enhancement to be made, which were averaged and the standard deviation was used as the uncertainty in the NOE enhancement.

The ^{1}H−^{15}N correlation spectra of CI2 and of CI2(20−59)•(60−83) are shown in Figure 3. Both spectra are well dispersed, making it relatively easy to measure the required peak heights. The cross-peaks from W24 and D64 are partially overlapped in intact CI2; the same is true for K43 and L68 in the complex. Consequently, the relaxation parameters of these residues may have greater errors than those of the remaining residues. In the spectrum of CI2, the cross-peak for K21 was too weak to enable accrate relaxation measurements to be made; relaxation data have not been included for this residue.

RESULTS

Data from CI2. The relaxation data measured for CI2 together with the T_1/T_2 ratio are shown in Figure 4. The T_1/T_2 ratio is fairly constant across the sequence of CI2, allowing a good initial estimate for τ_M to be made from the average ratio of 2.64 ± 0.04; τ_M is estimated as 4.76 ± 0.07 ns. Using this value of τ_M, only one residue, 58, required the inclusion of an exchange contribution to be able to fit the data satisfactorily. All the data, with the exception of the T_2 value for residue 58, were used in a grid search producing an optimized estimate for τ_M of 4.77 ± 0.02 ns. This value of τ_M was used to extract the Lipari and Szabo parameters shown in Figure 5. The high precision with which τ_M has been determined allows both the magnitudes and the trends in the model parameters to be interpreted. The trend in the order parameters confirms that, with the exception of the loop region between residues 55 and 66, the backbone is highly constrained. The constrained regions of the protein have an average S^2 of 0.90 ± 0.02, which is comparable to that of constrained residues in other proteins. The minimum order parameter of a residue in the loop is

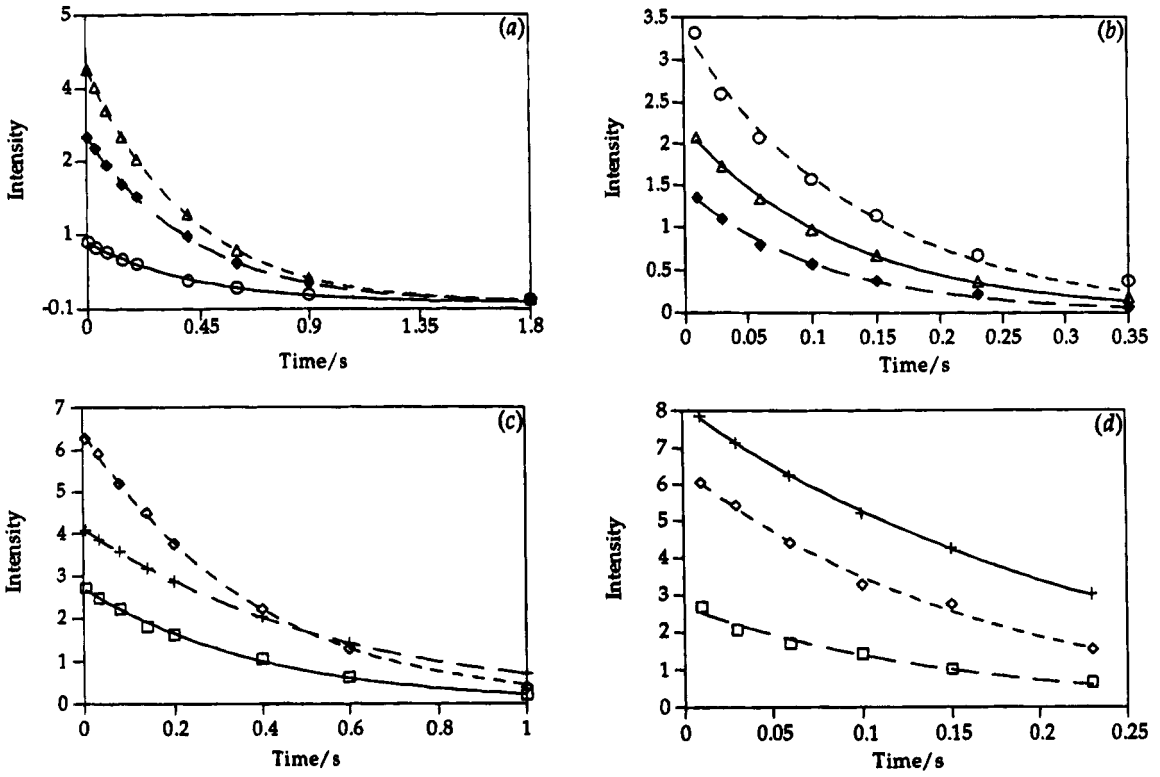

FIGURE 2: Plots showing the variation of cross-peak height as a function of time for selected residues during (a) the T_1 experiment and (b) the $T_{1\rho}$ experiment for CI2 and (c) the T_1 experiment and (d) the $T_{1\rho}$ experiment for CI2(30−51)•(60−83). Residues have been chosen which show the best fit (△, +), an average fit (◆, ◇), and the worst fit (○, □) to an exponential decay for CI2 and for CI2(20−59)•(60−83), respectively.

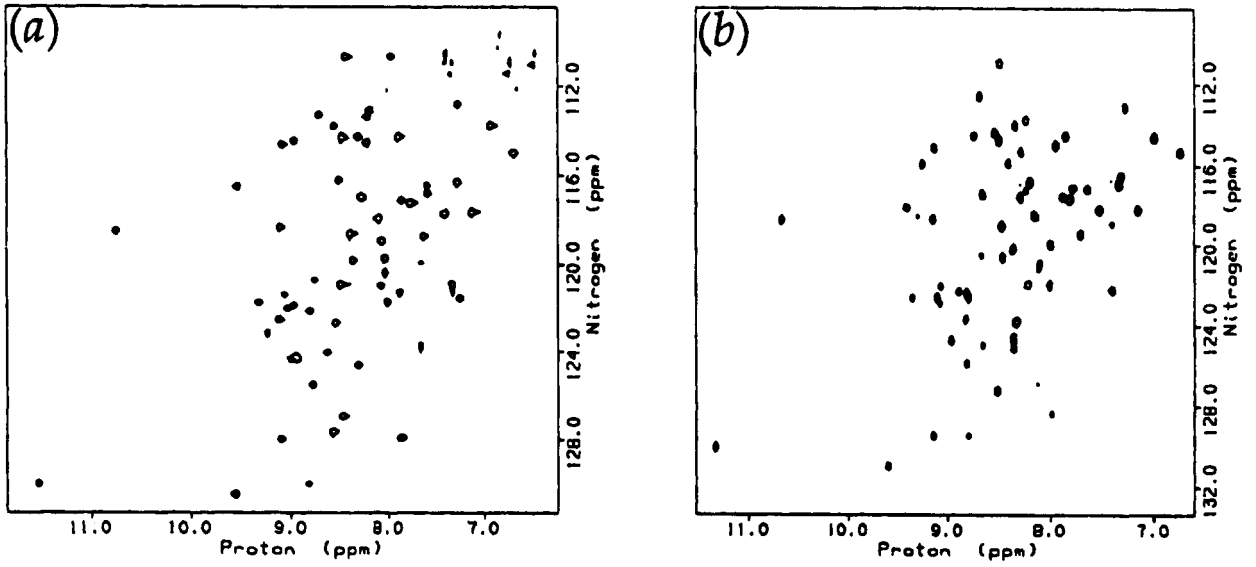

FIGURE 3: $^{15}N-^{1}H$ correlation spectra of (a) CI2 and (b) CI2(20−59)•(60−83) showing that most of the cross-peaks in these spectra are well resolved.

0.62 (residue 62), which indicates that even the loop is still quite constrained. This observation is consistent with features in the known structure; the loop is held down at one end by a hydrogen bond between residues T58 and R67 and at the other end by a salt bridge connecting residues R65, R67, and E60.

The trend in order parameters compares well with that obtained for eglin *c* (Peng & Wagner, 1992), which differs in sequence but is structurally and functionally very similar to CI2. Apart from the lack of a flexible N-terminus in CI2, residues 1−19 have been removed in this truncated form of CI2, the magnitudes of the order parameters also agree fairly well; the average S^2 for the structured regions of eglin *c* is 0.83. The difference arises because a slightly different N bond length was used in each calculation (1.03 Å in the present work and 1.02 Å in the case of eglin *c*); if a NH bond length of 1.02 Å is used in the analysis of the data from the CI2 work, the average S^2 is 0.87, which agrees, within the limits of experimental error, with that obtained for eglin *c*. The average internal correlation time for the constrained regions of CI2 is 100 ± 60 ps, which is consistent with those found in eglin *c* and other similar proteins.

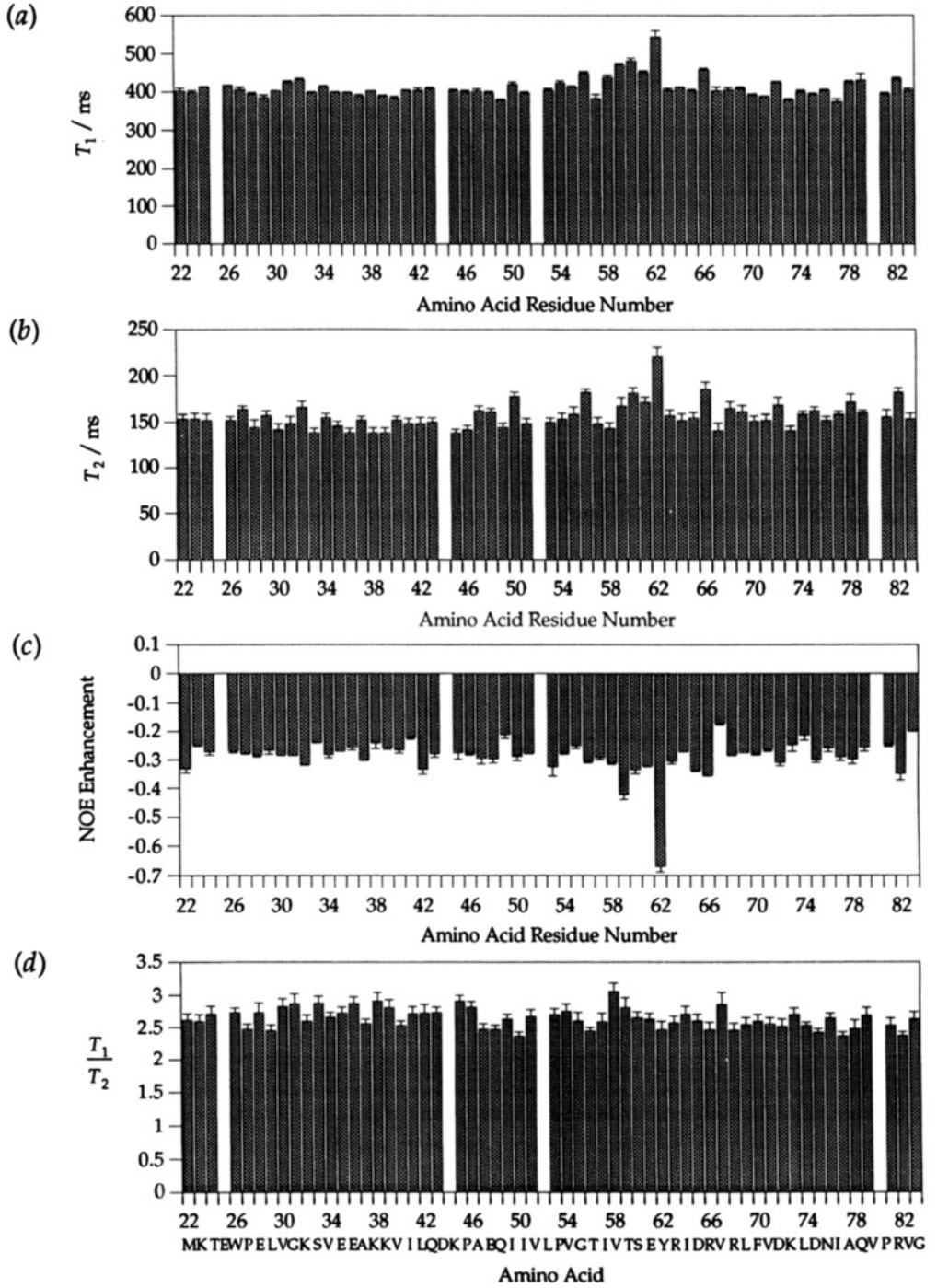

FIGURE 4: Plots showing (a) T_1, (b) T_2, (c) the $\{^1H\}-^{15}N$ NOE enhancement, and (d) the T_1/T_2 ratio for the backbone ^{15}N nuclei in CI2. The protein sequence for CI2 has been included in panel d.

Data from CI2(20−59)·(60−83). The relaxation data for the complex are presented in Figure 6. The T_1/T_2 ratio is fairly constant across the sequence, allowing a good initial estimate of τ_M to be made; the average T_1/T_2 ratio was 2.43 ± 0.04, giving an initial estimate for τ_M of 4.42 ± 0.07 ns. Using this correlation time, only residue 46 required the inclusion of an exchange contribution. The value of τ_M was optimized in the manner described previously, omitting the T_2 value of residue 46, to give a correlation time of 4.47 ± 0.03 ns. The order parameters and internal correlation times extracted using this value of τ_M are shown in Figure 7. The trend in S^2 indicates that the majority of the residues in the complex are well structured; the average S^2 for these regions is 0.90 ± 0.02, which agrees with that observed for CI2. The loop region appears to be substantially more mobile than in native CI2; the order parameters in the first half of the loop region (residues 53−59) decrease to 0.2, which is significantly lower than the minimum order parameter observed in the loop region of CI2. The second half of the loop (residue 60−64) has order parameters ranging from 0.57 to 0.92, indicating that although it is more mobile than the structured region of the protein, it is significantly less mobile than the first half of the loop.

The ^{15}N nucleus of residue 60 is present as an NH_2 in CI2(20−59)·(60−83), so no information concerning its mobility is obtained from these experiments. For the purposes of the following discussion it has been assumed, for convenience, that the mobility of residue 60 does not

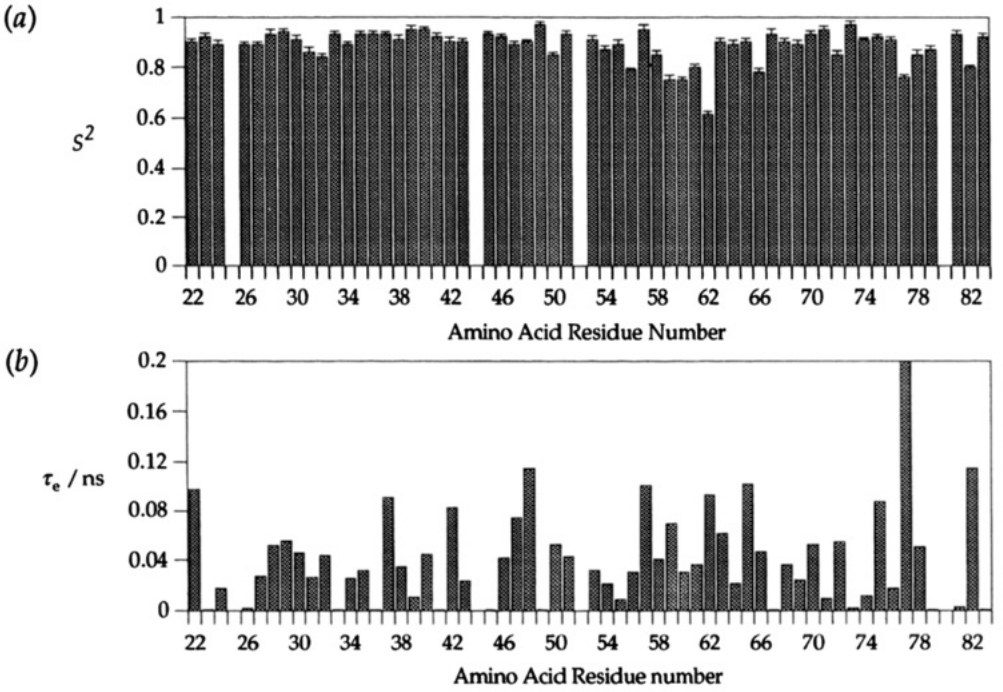

FIGURE 5: Order parameters and internal correlation times determined for CI2. Uncertainties in S^2 are the standard deviations taken from 500 Monte Carlo simulations.

differ significantly from that of residue 61. This assumption does not alter the conclusions of the following discussion since Glu60 is located on the end of a fairly constrained loop. Even if this residue were significantly more mobile than residue 61, its location in the protein structure is restricted by the this relatively rigid loop.

DISCUSSION

The order parameters and internal correlation times determined here reflect mobility in the high-frequency range, *i.e.*, on a time scale that is faster than the overall tumbling; much slower internal motions will not affect the order parameters. Motions which occur on a time scale slower than overall tumbling may introduce exchange contributions to T_2. Only one residue in the complex required an exchange contribution to T_2 so there is no evidence in the relaxation data to suggest that these slow motions are occurring, although the lack of a large number of exchange contributions does not necessarily imply that slow motions do not occur.

Motions occurring on a time scale slower than those which can be detected using relaxation measurements can be identified by measuring NH exchange rates in D_2O solution. When CI2 is placed in D_2O at pD 6.3 at room temperature, it takes between 2 and 3 months for the NH protons to completely exchange with deuterium (B. Davis and D. Otzen, unpublished results). In contrast, at pD 4.6 at room temperature the NH protons of the complex exchange completely after 24−48 h. This indicates that there may be slow internal motions present in the complex which make the NH protons much more accessible to the solvent. It is possible that this increase in the NH exchange rate results from a slow exchange process in which the complex dissociates into its separate components, which subsequently undergo rapid exchange with the D_2O solvent. The dissociation rate constant of the complex is approximately 0.0005 s^{-1} (Prat Gay et al., 1994), which is consistent with the observed NH exchange rates.

Comparison with RNase S. It is interesting to note that in the case of RNase S, the product of subtilisin clipping of RNase A, no electron density is observed in the electron density map obtained from crystallographic studies for residues 16−23 after cleavage of the peptide bond between residues 20 and 21 (Kim et al., 1992). Disruption of the native structure is more extensive on the N-terminal side of the cleavage point than the C-terminal side, analogous to the results obtained for CI2(20−59)•(60−83). However, NMR assignments for the loop 14−24 of RNase S are indicative of a random coil conformation on both sides of the cleavage point (J. Neira, personal communication). In contrast to RNase S, where the entire loop between two elements of secondary structure (helices A and B) is disrupted by cleavage, only the loop on the N-terminal side of the cleavage site is substantially disordered in CI2(20−59)• (60−83). Residues 60−64, which are not in a secondary or tertiary structure element, are relatively ordered.

The Loop Region. The large increase in mobility which accompanies the loss of a covalent bond is to be expected. It is noteworthy that it is the N-terminal region of the loop, residues 54−59, which is the most mobile, although the C-terminal region of the loop, residues 60−64, is somewhat more mobile than the rest of the protein. This may provide a model of the mechanism of inhibition of serine proteases by CI2.

The results discussed above indicate that, in the absence of an bound enzyme, cleavage of the scissile bond Met59−Glu60 results in the loop region 54−59 becoming disordered, while the loop region 60−64 remains relatively ordered. The interactions between 60−64 and the protein scaffold are therefore sufficient to prevent this region of the loop from adopting a random coil conformation when the scissle bond is cleaved. This loop region undergoes no significant conformational change when the inhibitor is bound to subtilisin (McPhalen *et al.*, 1985), and it is probable that interactions between residues 60−64 and the protein scaffold

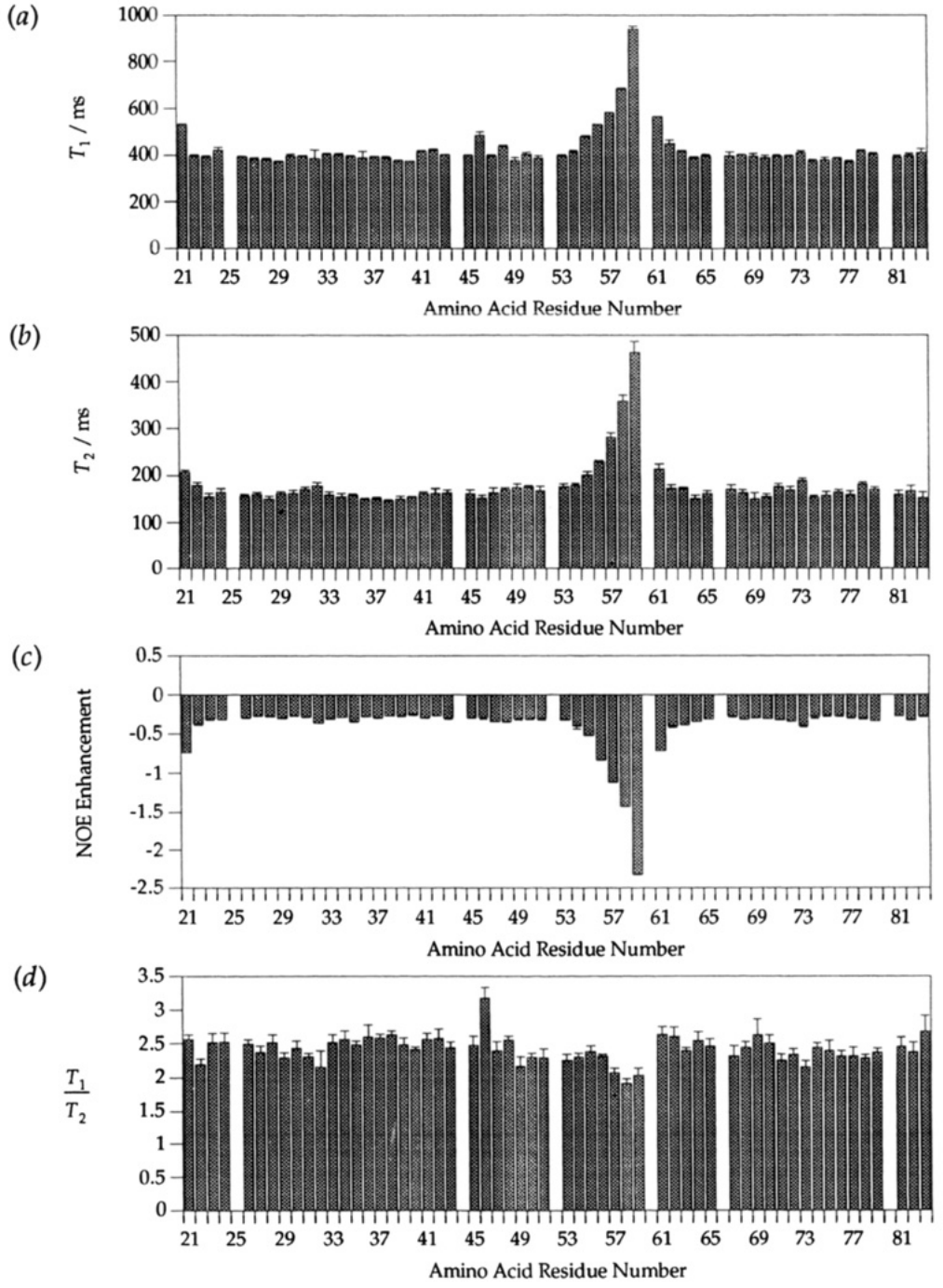

FIGURE 6: Plots showing (a) T_1, (b) T_2, (c) the $\{^1H\}-^{15}N$ NOE enhancement, and (d) the T_1/T_2 ratio for the backbone ^{15}N nuclei in CI2(20−59)•(60−83).

are similar in both the enzyme−inhibitor complex and the free cleaved inhibitor. Initial structural data (B. Davis, unpublished results) suggest that residues 60−64 do adopt a native-like conformation in CI2(20−59)•(60−83).

In the enzyme−inhibitor complex, the relative rigidity of the region 60−64 after cleavage of the scissile bond would leave the free amine group of Glu60 well placed to attack the acyl-enzyme intermediate; this favorable positioning would be enhanced by interactions made by the residue at position 61 with subtilsin. An equilibrium between the acyl-enzyme intermediate and the intact inhibitor would strongly favor the intact inhibitor (Longstaff et al., 1990) and would result in inhibition of the protease.

While the CI2(20−59)•(60−83) system is a useful model for the mechanism of inhibition of serine proteases by CI2, it must be stressed that significant differences exist between the cleaved species discussed here and the intact inhibitor bound to a protease.

Residue 59 has been chemically altered to a homoserine residue, which, as discussed below, is predominantly in the lactone isomer. This is structurally dissimilar to the methionine residue present in the intact protein. However, in the CI2(20−59)•(60−83) complex, residues 54−59 do not interact with the protein scaffold, and the modification of residue 59 is unlikely to have any effect on the results discussed here.

The CI2(20−59)•(60−83) species studied here is not bound to a protease. Numerous interactions are made between the loop region of CI2, residues 54−64, and subtilisin (McPhalen *et al.*, 1985). These interactions cannot be accounted for in

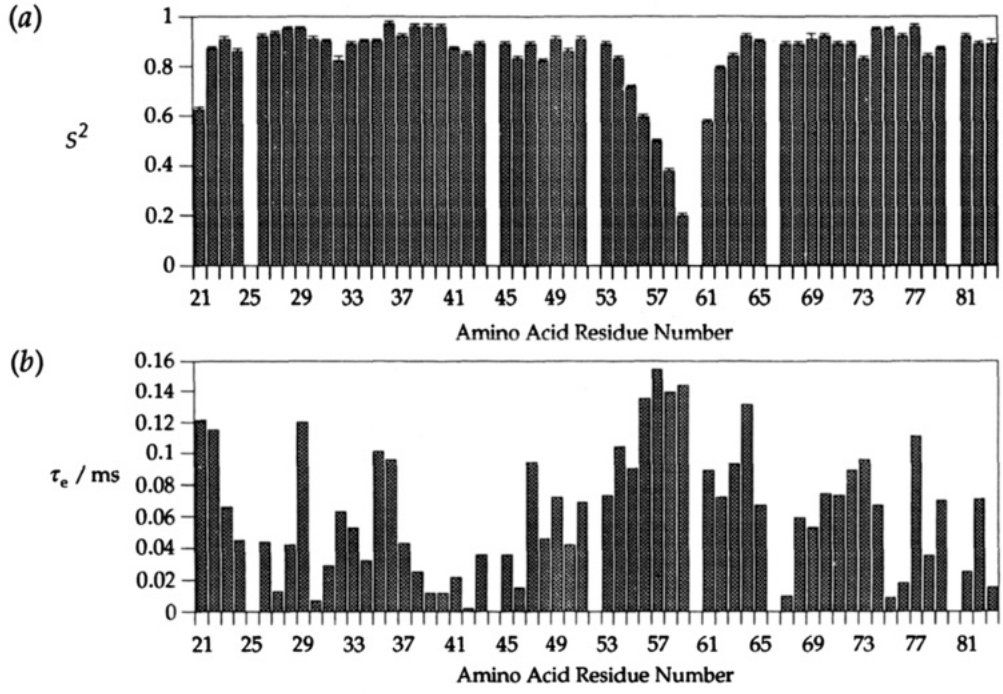

FIGURE 7: Order parameters and internal correlation times determined for CI2(20−59)•(60−83). The uncertainties in S^2 were calculated in the manner described for CI2.

this model. This system can only model interactions between the loop region, residues 54−64, and the protein scaffold of CI2 to which the loop is attached. These interactions appear sufficient to constrain residues 60−64 into a non random coil conformation and may be important in the inhibition of serine proteases by CI2.

The Nature of Hse59. CNBr cleavage of a protein initially generates a homoserine lactone in place of the methionine residue where cleavage occurs. This lactone can undergo mild alkaline hydrolysis to give the homoserine carboxylate (Kim et al., 1982). Isomers of Hse have been shown to produce conformational changes in small peptides (Kim et al., 1982), and the nature of Hse59 is therefore an important issue. CNBr cleavage was carried out at pH 2.3, and all subsequent experiments were performed at pH 4.6. Alkaline hydrolysis of the homoserine lactone should therefore be slowed, and the homoserine carboxylate isomers form only a small fraction of the population. Consistent with this are the observations that only one set of resonances is observed for Hse59 (B. Davis, unpublished data), and an NOE is observed between Hse59Hα and Hse59Hγ, indicative of the lactone isomer. Mass spectrometry data obtained for CI2-(20−59) in water showed the major population to be the lactone form, with only a small amount of the hydrolysis product present (J. Ruiz-Sanz, unpublished data). It is therefore reasonable to assume that, under the conditions used for the NMR experiments, the dominant homoserine isomer is the lactone.

Conclusion. The proposed mechanism of inhibition of serine proteases by CI2 (Longstaff et al., 1990), in which the scissile bond is re-formed by nucleophilic attack of the released amine of Glu60 on the acyl-enzyme intermediate, is strongly supported by these results. The region E60−D64 is substantially more ordered than the region G54−M59 in the complex formed after cleavage of the scissile bond. Interactions of Y61 with subtilisin would further restrain this loop.

ACKNOWLEDGMENT

We thank Dr. Prat Gay and Dr. Mark Bycroft for helpful discussions.

SUPPLEMENTARY MATERIAL AVAILABLE

Two tables containing experimental and calculated T_1, T_2, and NOE enhancements along with the calculated values of S^2 and τ_e for both CI2 and CI2(20−59)•(60−83) (4 pages). Ordering information is given on any current masthead page.

REFERENCES

Abragam, A. (1961) *Principles of Nuclear Magnetism*, Oxford University Press, Oxford.

Hiyama, Y., Niu, C., Silverton, J. V., Bavoso, A., & Torchia, D. A. (1988) *J. Am. Chem. Soc. 110*, 2378−2383.

Jackson, S. E., Moracci, M., elMasry, N., Johnson, C. M., & Fersht, A. R. (1993) *Biochemistry 32*, 11259−11269.

Kay, L. E.; Torchia, D. A., & Bax, A. (1989) *Biochemistry 28*, 8972−8979.

Kim, P. S., Bierzynski, A., & Baldwin, R. L. (1982) *J. Mol. Biol. 162*, 187−199.

Kim, E. E., Varadarajan, R., Wyckoff, H. W., & Richards, F. M. (1992) *Biochemistry 31*, 12304−12314.

Kraulis, P. J. (1991) *J. Appl. Crystallogr. 24*, 945−949.

Laskowski, M., Jr., & Kato, I. (1980) *Annu. Rev. Biochem. 49*, 593−626.

Lipari, G., & Szabo, A. (1982a) *J. Am. Chem. Soc. 104*, 4559−4570.

Lipari, G., & Szabo, A. (1982b) *J. Am. Chem. Soc. 104*, 4546−4559.

Longstaff, C., Campbell, A. F., & Fersht, A. R. (1990) *Biochemistry 29*, 7339−7347.

Luvwigsen, S., Shen, H., Kjaer, M., Madsen, J. C., & Poulsen, F. M. (1991) *J. Mol. Biol. 222*, 621−635.

Marion, D., Ikura, M., & Bax, A. (1989) *J. Magn. Reson. 89*, 425−430.

McPhalen, C. A., & James, M. N. G. (1987) *Biochemistry 26*, 261−269.

McPhalen, C. A., Svendsen, I., Jonassen, I., & James, M. N. G. (1985) *Proc. Natl. Acad. Sci. U.S.A. 82*, 7242−7246.
Osmark, P., Sorensen, P., & Poulsen, F. M. (1993) *Biochemistry 32*, 11007−11014.
Palmer, A. G., III, Cavanagh, J., Wright, P. E., & Rance, M. (1991) *J. Magn. Reson. 93*, 151−170.
Peng, J. W., & Wagner, G. (1992) *Biochemistry 31*, 8571−8586.
Prat Gay, G. de, & Fersht, A. R. (1994) *Biochemistry 33*, 7957−7963.
Prat Gay, G. de, Ruiz-Sanz, J., & Fersht, A. R. (1994) *Biochemistry 33*, 7964−7970.
Press, W. H., Teukolsky, S. A., Vetterling, W. T., & Flannery, B. P. (1992) *Numerical Recipes in FORTRAN*, 2nd ed., Cambridge University Press, Cambridge.
Shaka, A. J., Keeler, J., Frenkiel, T., & Freeman, R. (1983) *J. Magn. Reson. 52*, 335−338.
Stone, M. J., Fairbrother, W. J., Palmer, A. G., III, Reizer, J., Saier, M. H., Jr., & Wright, P. E. (1992) *Biochemistry 31*, 4394−4406.
van Mierlo, C. P. M., Darby, N. J., Keeler, J., Neuhaus, D., & Creighton, T. E. (1993) *J. Mol. Biol. 229*, 1125−1146.

BI941920V